An Effective Islanding Detection Method With Wavelet-Based Nuisance Tripping Suppressing

Marouane El Azzaoui

***Abstract*—The reactive power control (RPC) technique is a hopeful solution for the islanding issue in distributed generation (DG). Existing RPC approaches have downsides of inhibiting the required load reactive power or injecting/drawing undesirable excessive reactive power into the utility during normal operation. To overcome these limitations, the positive sequence voltage of point common coupling (PCC) is included in the reference of reactive power, which helps the frequency to deviate rapidly outside its thresholds. Further, power system transients which considered normal events can drift the frequency and result in a false islanding detection. In this article, different operating conditions such as load switching, voltage variations, and faults are considered. To address this issue, the suggested strategy includes a second decision-making criterion based on the discrete wavelet transform of the subtraction of sensed and nominal positive sequences of the PCC voltage. Simulation and experimental findings show that the suggested islanding detection method detects islanding rapidly and with zero nondetection zone. Furthermore, the DG and load reactive powers are closely matched under normal operation, and nonislanding situations are successfully prevented.**

***Index Terms*—Distributed generation (DG), fault detection zone (FDZ), islanding detection, nondetection zone (NDZ), reactive power control (RPC), wavelet transform.**

I. Introduction

RECENTLY, several distributed generation (DG) are penetrated into the power system due to the environment-friendly nature of renewable sources such as photovoltaic and wind turbine. The DG and its local load will be isolated from the grid when a fault occurs upstream of the utility grid. This situation results in the autonomous operation of the DG, which calls for safety issues to the appliances and personnel. Therefore, timely detection of islanding is highly required [1]. According to the IEEE Std. 1547-2018, islanding must be detected within 2 s of its formation.

Many approaches are proposed for islanding detection, including passive, active, and communication-based methods. The passive method is based on measuring the system's local parameters, e.g., the frequency and voltage. This method does not affect the normal operation of the system, and it is simple to perform. However, the choice of an appropriate threshold and the significant nondetection zone (NDZ) are unavoidable. The popular passive methods include over/under voltage protection (OVP/UVP), over/under frequency protection (OFP/UFP), rate of change of frequency, rate of change of power, and phase jump [2], [3]. The active method entails injecting a perturbation and monitoring the system's response. The advantage of this strategy is the small NDZ, and its limit is the power quality degradation [4]. The most common active approaches include Sandia and active frequency shift, and slip-mode frequency shift [5]. The communication-based strategy relies on the direct communication between the utility grid and the DG and can overcome the problems associated with passive and active techniques. The sole disadvantage is the high cost of installation [6]. In the literature, other works developed a hybrid technique [7], [8] that combines passive and active strategies to solve their drawbacks. Nonetheless, it brings additional complexity to the installation. Other works use artificial intelligence such as neural networks, fuzzy logic, and machine learning to detect islanding [9]–[11].

Most active detection systems introduce a current disturbance into the controller, causing voltage distortion. Among active techniques, the methods based on varying reactive power or reactive power control (RPC) are effective in shifting the frequency to cross its thresholds. Moreover, there is no distortion related to changes in reactive power, making it preferable to other approaches [12]. Further, it proved that the RPC is more cost-effective than the active power control in islanding detection [13]. The RPC method is discussed in [14] and [15]. It is based on establishing reactive power mismatch to deviate the frequency outside its thresholds after islanding. The RPC approach can quickly detect islanding without NDZ.

In the RPC approach presented in [14], the reactive power is assumed to be zero in normal operating conditions. In this instance, the DG does not generate the reactive power to meet the load's needs. However, the method [15] injects additional reactive power into the grid during normal operation. In addition, nonislanding events, e.g., load connection/disconnection, voltage variations, and faults, can also create a false islanding detection by deviating the frequency. To tackle these setbacks, a strategy based on the phase angle between sensed and nominal voltages at the PCC bus is proposed in [16].

However, due to its complexity, no experimental findings are offered. To address the previously mentioned concerns, this work presents a modified RPC strategy for robust islanding detection. First, to achieve a fast islanding detection and avoid

Manuscript received December 4, 2020; revised March 20, 2021; accepted May 27, 2021. Date of publication June 9, 2021; date of current version August 16, 2021. Recommended for publication by Associate Editor Prof. H. H.-C. Iu.

The author is with the LISAD Laboratory, Department of Industrial Engineering, National School of Applied Sciences of Agadir, Ibn Zohr University, Agadir 80000, Morocco (e-mail: m.elazzaoui@uiz.ac.ma).

Color versions of one or more figures in this article are available at https://doi.org/10.1109/TPEL.2021.3087915.

Digital Object Identifier 10.1109/TPEL.2021.3087915

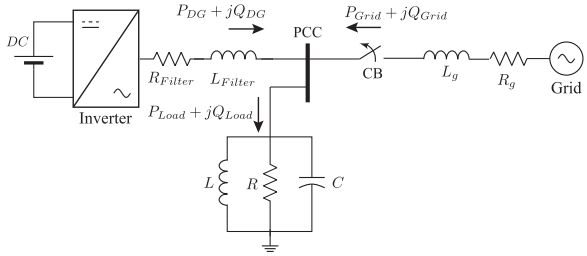

Fig. 1. Islanding test setup.

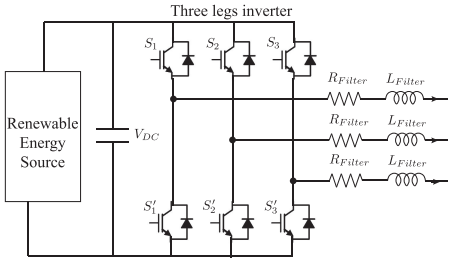

Fig. 2. Topology of the inverter.

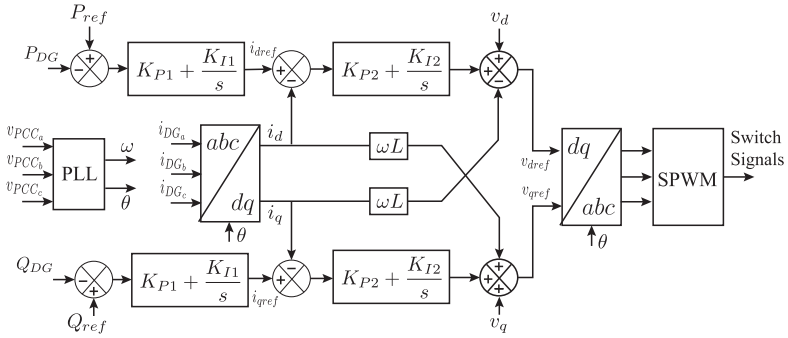

Fig. 3. Block diagram of the DG interface control.

additional reactive power injection, the reference of the reactive power is expressed in terms of the positive sequence and the frequency of the PCC voltage. Afterward, as previously stated, any disturbance might cause frequency deviation, yielding to false islanding detection. To address this critical issue, DWT of the subtraction of measured and nominal positive sequence of the PCC voltage is considered to ensure a second-level decision-making criterion for islanding detection.

This article makes the following contributions.

1) Designing an RPC islanding strategy for DG systems to satisfy the local loads' requirement regarding reactive power during normal operation.
2) Introducing a wavelet technique to distinguish between islanding and nonislanding events

The originality of the suggested islanding detection method (IDM) is discussed in Sections III and IV, and validated with simulation and experimental findings in Sections V and VI.

II. System Under Study

The appropriate islanding test setup is depicted in Fig. 1 according to the IEEE Std. 1547-2018. It comprises a DG interface represented by a constant dc voltage and a three-phase inverter, a circuit breaker (CB), a parallel *RLC* load, and the main utility represented by a voltage source with impedance. The local load is usually linked close to the DG system, and the transmission length is relatively short. Thus, line losses are minimal, and the DG and *RLC* loads are linked at the PCC.

In the grid-tied mode, the DG is intended to operate as a constant power source controlling the active and reactive powers independently using dual closed loop in the *d–q* synchronous reference frame. A two-level inverter is used in this study, and its topology is presented in Fig. 2. Fig. 3 illustrates the block diagram of the DG interface control. It consists of three main parts that are; the phase-locked loop (PLL), the inner current control loop, and the outer power control loop. The PLL is used to calculate the voltage phase angle to achieve Park transformations and estimate the frequency of the PCC voltage. For the inner control loop, proportional-integral (PI) regulators are introduced to minimize the error between the measured and reference current in the *d–q* synchronous frame. Similarly, for the outer control loop, PI regulators are used to minimize the error between the measured and reference active and reactive powers. The *d–q* reference voltages in the output of the inner current control loop are transformed to abc reference voltages using inverse Park transformation. Then, the triggering signals to drive the inverter are obtained by sinusoidal pulsewidth modulation (SPWM).

As illustrated in Fig. 1, when the DG is attached to the grid, the powers are given by the following formulas:

$$P_{\text{Load}} = P_{\text{DG}} + P_{\text{Grid}} = 3\frac{V_{\text{PCC}}^2}{R} \tag{1}$$

$$Q_{\text{Load}} = Q_{\text{DG}} + Q_{\text{Grid}} = 3V_{\text{PCC}}^2\left(\frac{1}{2\pi fL} - 2\pi fC\right) \tag{2}$$

with f and V_{PCC} are the frequency and voltage at the PCC bus, and R, L, and C are the components of the *RLC* load. Moreover, the resonant frequency f_0 and quality factor Q_f are given by [17]

$$Q_f = R\sqrt{\frac{C}{L}} = 2\pi f_0 RC \tag{3}$$

$$f_0 = \frac{1}{2\pi\sqrt{LC}}. \tag{4}$$

The worst case of islanding detection is when $Q_f = 1$ as specified by IEEE 1547 standards, and f_0 equal the grid frequency [18]. By merging (1)–(4), Q_{Load} can be expressed as:

$$Q_{\text{Load}} = P_{\text{Load}}.Q_f\left(\frac{f_0}{f} - \frac{f}{f_0}\right). \tag{5}$$

If P_{Grid} is not zero when the circuit breaker is opened, and the grid is disconnected, the PCC voltage will grow or drop during the islanding event due to the active power mismatch $\Delta P = P_{\text{DG}} - P_{\text{Load}}$. The magnitude of the voltage variation is determined by the power imbalance. Using the OVP/UVP approach, this variation may be detected. The active power

mismatch can be expressed as [19]

$$\Delta P = P_{\text{DG}} \left(1 - \frac{1}{(1+\Delta V)^2}\right) \tag{6}$$

with ΔV is given by

$$\Delta V = \frac{V'_{\text{PCC}} - V_{\text{PCC}}}{V_{\text{PCC}}} \tag{7}$$

with V_{PCC} and V'_{PCC} are the voltages at the PCC bus before and after islanding event, respectively.

Likewise, (2) indicates that the amount of frequency variation is driven by both active and reactive power mismatches. The OFP/UFP approach can be used to identify this frequency variation. If reactive power mismatch equals zero before islanding, the active power mismatch during islanding will affect the reactive power usage, permitting frequency variation. In addition, the reactive power imbalance will cause the frequency to shift. The reactive power imbalance $\Delta Q = Q_{\text{DG}} - Q_{\text{Load}}$ is given by

$$\Delta Q = P_{\text{DG}} R \left(\frac{1}{2\pi L}\left(\frac{\Delta f}{f^2 + f.\Delta f}\right) + 2\pi \Delta f C\right) \tag{8}$$

with Δf is given by

$$\Delta f = f' - f \tag{9}$$

with f and f' represent the frequency at the PCC bus before and after the islanding condition, respectively.

With close matched power, the frequency and voltage variations are too small to trip over/under voltage (OUV)/over/under frequency (OUF) system protection, leading to large NDZ [20]. The next section discusses islanding detection by drifting the frequency over its thresholds.

III. Proposed Islanding Detection Method

To identify islanding, a modified Q–f droop approach is utilized in this research. In the grid-tied mode, the frequency is imposed by the utility. Once islanding occurs, the frequency variation will depend on the reactive components of the load. According to (2), if the reactive power mismatch exists before islanding, the frequency will shift until the load's reactive power matches the DG reactive power. If the DG reactive power is set to zero to feed the unitary power factor, this frequency matches the resonant frequency of the load determined in (4). Since the resonant frequency is given in terms of L and C, multiple combinations might result in a resonant frequency in the OFP/UFP range. Based on the IEEE Std. 1547-2018, the voltage thresholds range from 88% to 110% and the frequency from 49.3 to 50.5 Hz (50 Hz is the rated frequency of the grid). For a load resonating between 49.3 and 50.5 Hz, the PCC frequency will remain in this range (49.3–50.5 Hz). In this situation, this loading condition is regarded within the NDZ. For a load with 5-kW rated active power and the quality factor $Q_f = 1.0$, the nonlinear relation between load reactive power and frequency given in (5) is illustrated in Fig. 4. The Q–f characteristic can be represented by a linear characteristic between the frequencies 49.3 and 50.5 Hz, and it has a negative slope. In [14], the DG's reactive power was assumed to be zero, while in this work, the load's reactive power is compensated by the DG after the islanding event. Thus, the DG reactive power denoted Q_{ref} is represented by a horizontal line in the Q–f curve as shown in Fig. 4 for $Q_{\text{ref}} = 0$ Var. Three loads with resonance frequencies of 49.3, 50, and 50.5 Hz are shown in Fig. 4. The frequency after islanding is determined by the intersection of the DG and load Q–f curves, which indicates that a load with a resonance frequency of 50.5 Hz will stabilize at point C in the islanding mode.

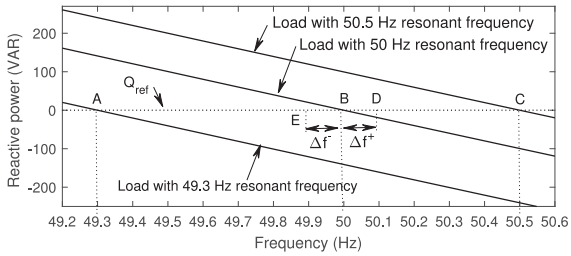

Fig. 4. Q–f curve with 5-kW rated power, $Q_f = 1.0$, and $Q_{\text{ref}} = 0$ Var.

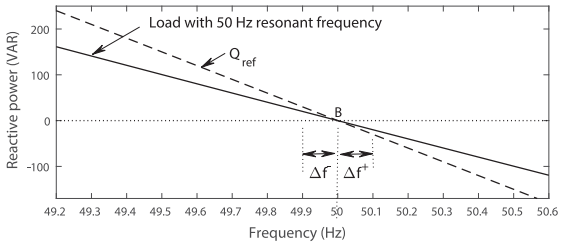

Fig. 5. Q–f curve with frequency variation.

The three examples in Fig. 4 are all within the NDZ and are undetectable by the OFP/UFP technique. Furthermore, any load having a resonance frequency between A and C is regarded as undetectable. In this situation, the operating points A, B, and C are all deemed stable. To determine the stability of each point, the reactive power mismatch is computed for a slight variation of the frequency to the right and left, as depicted in Fig. 4. The reactive power mismatch $\Delta Q = Q_{\text{DG}} - Q_{\text{Load}}$ will be negative for a tiny positive frequency variation Δf^+. Thus, the frequency will drop after islanding to increase the load's reactive power [refer to (5)], and the point D will tend toward point B. Likewise, the reactive power mismatch will be positive for a tiny negative frequency variation Δf^-. Thus, the frequency will rise after islanding to decrease the load's reactive power, and the point E will be moved to point B. As a result, whether the frequency deviation is positive or negative, the frequency will stabilize at point B, which is regarded as a stable operating point.

To make the operating points A, B, and C unstable, the DG reactive power is designed to have a greater negative slope than the reactive power of the loads as presented in Fig. 5. All load Q–f curves, regardless of the resonant frequency, have the same shifted slopes. Q_{ref} has been stated by Zeineldin [14] as follows:

$$Q_{\text{ref}} = -k1 \times f + k2. \tag{10}$$

where k_1 and k_2 are positive values that must be selected to guarantee a greater DG slope than all load slopes between 49.3 and 50.5 Hz range.

By applying the same idea highlighted in Fig. 4, the point B presented in Fig. 5 would be unstable when the DG is equipped with Q_{ref} characteristic. The reactive power of the load decreases for a slight positive frequency variation, and the frequency will rise and diverges away from the point B until crossing the higher threshold limit (50.5 Hz). On the other hand, the reactive power increases with a tiny negative frequency change, and the frequency will fall and shifts away from the point B until overtaking the lower threshold limit (49.3 Hz).

It is apparent from (10) that the DG reactive power is zero before islanding to ensure a unitary power factor. Nevertheless, the DG with RPC contributes to voltage support and power factor improvement. The DG's Q_{ref} is equal to the load reactive power Q_{Load} in this scenario. Hence, the reactive power imbalance is zero after the islanding event. Chen and Li [15] have proven that the frequency variation induced by active and reactive power mismatches will be compensated by each other if ΔP and ΔQ have the same signs, yielding to slow islanding detection. In contrast, if ΔP and ΔQ have opposite signs, the frequency variation will be considerable, leading to quick islanding detection. Chen and Li [15] also proposed a modified RPC islanding detection, where Q_{ref} is defined as

$$Q_{\text{ref}}=\begin{cases}-\left(k_1+\frac{V_{\text{PCC}}-V_N}{V_N}\times k_2\right)(f-a)+Q_{\text{Load}}, V_{\text{PCC}}\geq V_N\\ -\left(k_1+\frac{V_N-V_{\text{PCC}}}{V_N}\times k_2\right)(f-b)+Q_{\text{Load}}, V_{\text{PCC}}<V_N\end{cases} \tag{11}$$

where $a=49.2$ and $b=50.6$, and k_1, k_2 are positive values, V_{PCC} and f are the sensed voltage and frequency at the PCC bus, respectively, and V_N is the nominal voltage at the PCC bus. Referred to (11), the reference reactive power Q_{ref} varies based on the variation of V_{PCC}, f, and Q_{Load}. Even in normal operating conditions, the existence of a and b in (11) induces a reactive power imbalance between the DG and the load. In this case, the reactive power mismatch uselessly injects/draws reactive power into/from the grid. Thus, the purpose of the proposed IDM is to create a reactive power imbalance after islanding. The suggested reference reactive power is defined as

$$Q_{\text{ref}}=-k_1(f-50)+k_2\left(\frac{V_N-V_{\text{PCC}}^+}{V_N}\right)+Q_{\text{Load}}+k_3 \tag{12}$$

where k_1 and k_2 are positive values, k_3 is in Var used to detect islanding if $\Delta P=0$, and V_{PCC}^+ is the voltage positive sequence.

According to (12), the frequency will be 50 Hz during normal operation, and the sensed V_{PCC}^+ would equal V_N, because the grid sets the PCC voltage. The DG system will produce the reactive power to meet the load's requirements ($Q_{\text{ref}}=Q_{\text{Load}}$). During islanding event, if $\Delta P>0$, then $V_{\text{PCC}}^+>V_N$ and $f>50$ Hz [refer to (1) and (2)], and $\Delta Q<0$ resulting in quick detection time as described previously. Likewise, if $\Delta P<0$, then $V_{\text{PCC}}^+<V_N$ and $f<50$ Hz, and $\Delta Q>0$ leading also to rapid islanding detection. If $\Delta P=0$, then $V_{\text{PCC}}^+=V_N$ and $f=50$ Hz, and consequently $\Delta Q=k3>0$ allowing islanding detection. Hence, the suggested methodology includes two key elements, which are as follows:

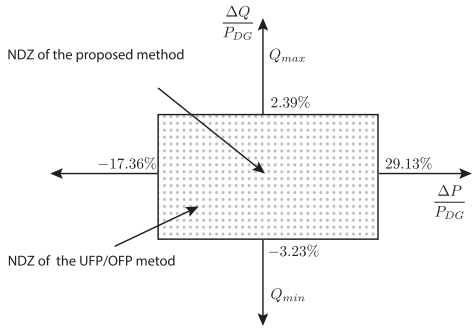

Fig. 6. NDZ of the proposed method and UFP/OFP.

1) creating reactive power mismatch after islanding not during normal operating conditions to eliminate the NDZ by forcing the frequency to diverge outside the thresholds;
2) ensuring frequency deviation consistency created by both active and reactive power to accelerate islanding detection.

A. NDZ Analysis

According to the IEEE std. 1547-2018, the PCC voltage thresholds range from 88% to 110%. Thus, the reactive power mismatch over DG active power ($\Delta Q/P_{\text{DG}}$) estimated using (6) for the UFP/OFP technique is -17.36% and 29.13%. The reactive power mismatch over DG active power ($\Delta Q/P_{\text{DG}}$) derived from (8) is -3.23% and 2.39%, with frequency cutoff limits ranging from 49.3 to 50.5 Hz and $Q_f=1$. As a basis, (6) and (8) may be used to calculate NDZ. Moreover, the NDZ of the UFP/OFP and the suggested techniques are shown in Fig. 6. The NDZ for the suggested approach is zero.

IV. Proposed IDM for Eliminating Nuisance Tripping

A. Transient Events

Any power system is concerned with transient phenomena caused by a system configuration or a change in operating conditions. Power system transients can be caused by load variations, lightning strokes, switching operations, large motor starting, faults, and even electromagnetic phenomena. These transients have different frequency, magnitude, and duration times according to the causes of transients. In general, an accurate calculation of transient is difficult even for small-scale systems because of the interaction between the components and the stochastic nature of transient. For most transients, an approximate solution can be obtained by simulation. The transient event generates high-frequency components that include plentiful information for a frequency range from dc to several kilohertz.

In accordance with the signal analysis of some power system transients, the simplified model of the transient can be expressed mathematically by the dumped equation shown in (13), and by the oscillatory dumped equation shown in (14) [21]. The noise is represented by Gaussian white noise

$$V_1=V_m e^{-\frac{t}{\tau}} \quad \text{or} \quad V_1=V_{m1}e^{-\frac{t}{\tau_1}}-V_{m2}e^{-\frac{t}{\tau_2}} \tag{13}$$

$$V_2 = V_m \sin(2\pi ft)e^{-\frac{t}{\tau}} \text{ or } V_2 = V_m \sin(2\pi ft)\left(e^{-\frac{t}{\tau_1}} - e^{-\frac{t}{\tau_2}}\right). \tag{14}$$

where τ, τ_1, and τ_2 are the time constants, and f is the frequency that depends on the nature of the transient.

For various operating conditions, IDM must be dependable. If a nonislanding event occurs, such as fault and load connection/disconnection [22], the frequency may exceed the thresholds range, resulting in false islanding detection. Thus, an extra constraint must be designed to enhance the robustness of the proposed IDM. The idea is to calculate the energy entropy using DWT of the voltage *V*, which is the subtraction of the PCC voltage's sensed and nominal positive sequence. The next section explores this idea to prevent false tripping.

B. Wavelet-Based Nuisance Tripping Eliminating

Let V the subtraction of sensed and nominal positive sequence voltages at the PCC bus

$$V = (V_{\text{pcc}}^{+})_{\text{sens.}} - (V_{\text{pcc}}^{+})_{\text{nom.}} \tag{15}$$

The proposed nuisance tripping detection is based on the Wavelet transform, which is a time- and frequency-domain signal processing for extracting characteristics from time-varying signals [23]. It is a series of functions used to analyze a signal in the time- and frequency-domain by decomposing it into its constituents at different frequency bands called wavelet coefficients [24]. The wavelet theory has been investigated in several works, including [25] and [26], and as a result, the next section provides a summary of the wavelet theory.

Continue wavelet transform (CWT) and discrete wavelet transform (DWT) are the two most common types of wavelet transforms. Despite this, the DWT is frequently utilized owing to its ease of implementation in digital signal processing, data compression capabilities, nonredundancy, and computational efficiency [27]. The CWT of the voltage V is given by [26]

$$W_{a,b} = \frac{1}{\sqrt{a}} \int_{-\infty}^{\infty} V(t)\psi\left(\frac{t-b}{a}\right) dt \tag{16}$$

where $\psi(.)$ is called mother wavelet, a is the scale or dilation factor, and b is the translation factor. This give a set of wavelet coefficients $W_a(t)$ for the level b [28].

The wavelet transform can be regarded as the convolution between the signal $V(t)$ and the wavelet kernel $\psi(t)$

$$W_a(t) = V(t) * \psi_a(t). \tag{17}$$

The result is a set of wavelet coefficients $W_a(t)$, and the wavelet $\psi_a(t)$ is dilated as

$$\psi_{a,b}(t) = \frac{1}{\sqrt{a}}\psi\left(\frac{t-b}{a}\right). \tag{18}$$

DWT is a useful technique when a time-varying signal must be investigated, as in transient events, where the time and frequency localization is needed. In 1988, Mallat used filter banks to design an effective DWT implementation technique (see Fig. 7) [28], [29]. This algorithm involves the wavelet and approximation kernels, denoted $\psi[n]$ and $\phi[n]$ (high- and low-pass finite impulse response filters, respectively), which are dilated by two in each scale. First, the discrete voltage signal $V[n]$ is convolved with the wavelet kernels $\psi(n)$ and $\phi(n)$, and downsampled by a factor of two to produce detail coefficient d_1 and approximation coefficient a_1. The functions $\psi[n]$ and $\phi[n]$ are applied to approximation coefficient a_1, and then, downsampled by a factor of two to generate the detail and approximation coefficient d_2 and a_2 for the second level. This procedure is repeated for *N* levels as shown in Fig. 7.

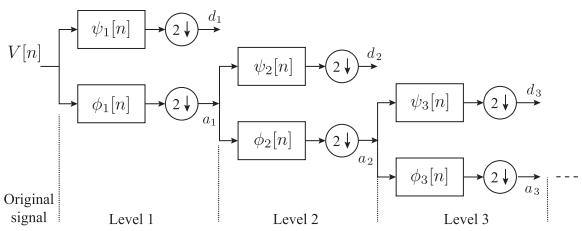

Fig. 7. Three levels DWT decomposition.

In the case of DWT, the mother wavelets are dilated by powers of two, giving rise to a set of child wavelets as [26]

$$\psi_{j,k}(t) = \frac{1}{\sqrt{2^j}}\psi\left(\frac{t-k2^j}{2^j}\right) \tag{19}$$

$$\phi_{j,k}(t) = \frac{1}{\sqrt{2^j}}\phi\left(\frac{t-k2^j}{2^j}\right) \tag{20}$$

where j and k are the scale and shift integer parameters, respectively. From Fig. 7, the detail and approximation coefficients are calculated by convolving the voltage signal with a series of high- and low-pass filters. For the three first levels, the coefficients are given by

$$d_1 = \psi_1 * V \tag{21}$$

$$d_2 = \psi_2 * \phi_1 * V \tag{22}$$

$$d_3 = \psi_3 * \phi_2 * \phi_1 * V \tag{23}$$

$$a_1 = \phi_1 * V \tag{24}$$

$$a_2 = \phi_2 * \phi_1 * V \tag{25}$$

$$a_3 = \phi_3 * \phi_2 * \phi_1 * V. \tag{26}$$

By generalizing for $j = 1$ to N levels, and adopting the symbol $\prod$ as serial convolution, (21)–(26) are represented as

$$d_1 = \psi_1 * V \tag{27}$$

$$d_j = \psi_j * \prod_{i=1}^{j-1}(\phi_i *)V \tag{28}$$

$$a_j = \prod_{j=1}^{N}(\phi_j *)V. \tag{29}$$

As mentioned before, the voltage V is selected as the signal to be assessed using DWT. Because of its compactness and localization capabilities in power system transients, the Daubechie's 3 (dB3) was chosen as the mother wavelet to extract features. Simulink environment was used to run multiple simulations utilizing the DWT decomposition with varied mothers wavelet

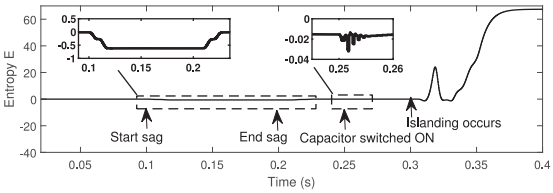

Fig. 8. Entropy of V during normal and islanding events.

and diverse load and fault conditions. The fourth-level wavelet coefficients are generated and utilized to extract the energy entropy which is included in decision-making criteria. From the approximation coefficients, the suggested energy entropy is determined as

$$E(V) = \sum_i a_i^2 \log\left(a_i^2\right). \tag{30}$$

To understand the proposed method, a numerical simulation was carried out at 50 kHz as sampling frequency using the DWT decomposition at level 4 of the Debauchies wavelet dB3, and the obtained findings are shown in Fig. 8. In this simulation, a 10% voltage sag starts at 0.1 s and ends at 0.2 s, and a capacitor bank is switched ON at 0.25 s, and the islanding condition is simulated at 0.3 s. As shown in Fig. 8, the energy entropy of the selected voltage is negative and very less during voltage sag and capacitor switching (normal events) when compared with the entropy during the islanding condition, which is very significant and takes positive values. With the voltage V and the proposed entropy expression, the magnitude of the entropy during normal events is always negative, while in the islanding condition, it takes positive values. Based on this observation, instead of tuning a threshold of entropy, it is clear that zero can be considered as a threshold to differentiate between normal and islanding events. Hence, a second decision criterion based on entropy is added to prevent false tripping, as presented in the flowchart of Fig. 9.

Islanding event will be identified when both the frequency and entropy conditions are verified. Nonetheless, suppose only the frequency criterion is fulfilled. The system will not issue a trip signal for the islanding relay since the frequency variation in this situation is generated by a regular event that represents a nuisance tripping.

C. Fault Detection Zone (FDZ) Analysis

Suppose a normal operation, if calculated entropy is less than the entropy threshold and the measured frequency is outside its thresholds, false islanding will be detected. In this case, DG falls within FDZ. To evaluate the risk of this approach to fall within the FDZ, the subtraction of the entropy E and its threshold $E_{\text{Threshold}}$ is defined as

$$\text{EF} = E - E_{\text{Threshold}} \tag{31}$$

where EF is called the entropy factor. A tiny EF denotes a circumstance where entropy under the islanding state is similar to entropy under a normal state, increasing the likelihood of dropping into the FDZ. To obtain a minimum FDZ, the entropy factor expressed in (31) is used to select an appropriate threshold.

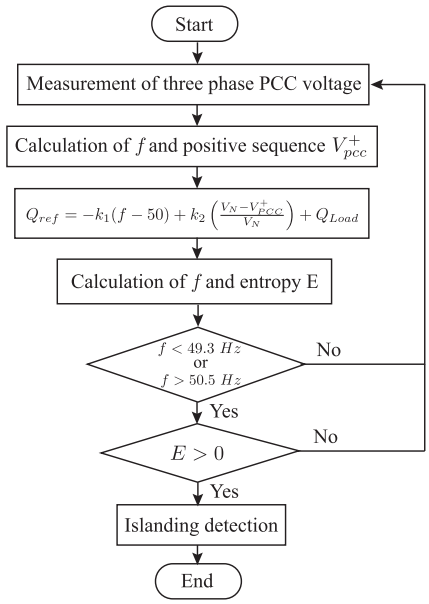

Fig. 9. Proposed islanding detection algorithm.

V. Simulation Results

In this section, several scenarios are simulated on MATLAB/Simulink based on the system in Fig. 1. The main parameters are summarized as follows : $P_{\text{DG}} = 5$ kW; $V_{\text{DC}} = 800$ V; $V_g = 220$ V; $L_g = 0.1$ mH; $R_g = 0.088\ \Omega$; $R = 29\ \Omega$; $L = 92.4$ mH; and $C = 110\ \mu$F. The performance of the proposed IDM is tested under various conditions.

A. Comparison of the Proposed Method With That Reported in [14] and [15]

The IDMs in [14] and [15] are also based on the RPC method. This subsection compares the suggested approach's performance to that of the previously discussed techniques. A simulation test with $\Delta P = 0$ and capacitor bank switching is carried out to compare their effectiveness. The capacitor bank is connected at 0.1 s and disconnected at 0.2 s, with islanding occurring at 0.3 s. Fig. 10 depicts frequency responses. For the reported methods in [14] and [15], once the capacitor is connected, the frequency surpasses the thresholds, yielding to false islanding as shown in Fig. 10(a) and (b). Furthermore, it should be noted that the second criterion based on entropy is not validated for the proposed technique, and its value is smaller than the threshold when the capacitor is connected/disconnected, as shown in Fig. 10(c). In this case, nonislanding events is identified as discussed in the flowchart of Fig. 9. However, once islanding occurs, both the frequency and entropy are validated, which can detect islanding. The detection time is 40 ms, which is within the specified value defined in the IEEE 1547 Standard.

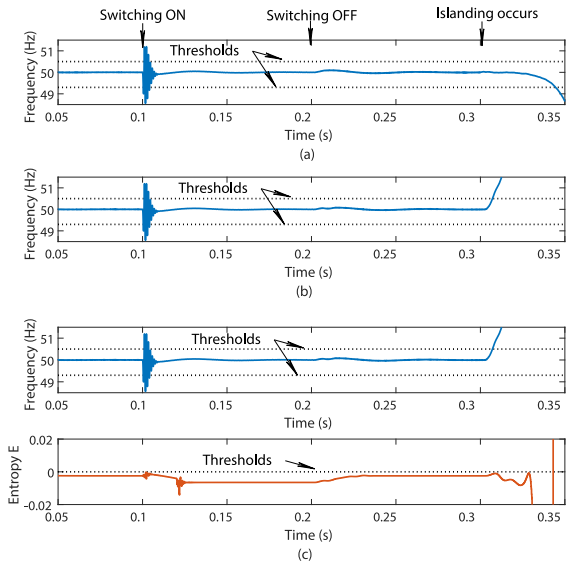

Fig. 10. Comparison of the proposed method with that reported in [14] and [15].

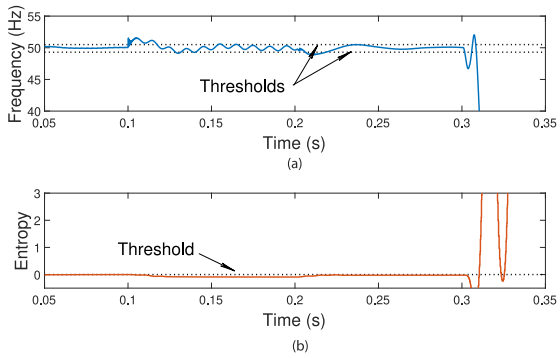

Fig. 11. Proposed IDM under multiple DG operation.

B. Performance of the Proposed IDM Under Multiple DG Operation

An additional DG is connected to the PCC bus to evaluate the performance of the proposed method under multiple DG operations. Both DGs are equipped with the proposed method. However, the RPC method for each DG should be modified as follows:

$$Q_{\text{ref}} = \begin{cases} -\left(k_1 + \frac{V_{\text{PCC}} - V_N}{V_N} \times k_2\right)(f-a) + C_p \times Q_{\text{Load}}, V_{\text{PCC}} \geq V_N \\ -\left(k_1 + \frac{V_N - V_{\text{PCC}}}{V_N} \times k_2\right)(f-b) + C_p \times Q_{\text{Load}}, V_{\text{PCC}} < V_N \end{cases} \quad (32)$$

where C_p represents the reactive power capacity of each DG in percent. To test the effect of connecting/disconnecting DG, one DG is already considered supplying the local load, while the second is connected at 0.1 s and disconnected at 0.2 s. In this test, a synchronization phase error of 10° when connecting the second DG is considered. Fig. 11 presents the frequency of the PCC bus and entropy obtained. It is observed from Fig. 11(a) that

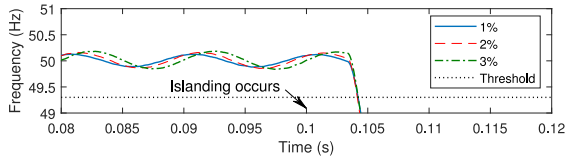

Fig. 12. Test of IDM under imbalanced loads.

when the second DG is connected, the frequency is destabilized and crossed the threshold limits. In this situation, false islanding is detected by considering the method of [15]. However, By examining Fig. 11(b), the entropy is decreased when the second DG is connected and did not exceed the threshold, which is fixed at zero. Thus, the second criterion based on entropy prevents false islanding detection. On the other hand, when islanding occurs, both frequency and entropy conditions are satisfied, and islanding is detected.

C. Test of the Proposed IDM Under Imbalanced Load

Imbalanced load is a common occurrence caused by various factors, including imbalanced impedance in distribution or transmission lines and connection/disconnection of a three-phase heavy load. As a result, the impact of an imbalanced load on the proposed IDM is analyzed. Fig. 12 shows the response of the frequency for three imbalanced loads: 1%, 2%, and 3%, when the islanding condition occurs at 0.1 s. The frequency deviates from the threshold limits in all three circumstances. Furthermore, the detection times are nearly identical in all three scenarios. As a result, the suggested IDM can successfully identify islanding under imbalanced load settings.

D. Performance of the IDM During Load and DG Switching

To evaluate the performance of the proposed IDM under various switching events, an additional linear load (resistive, inductive, and capacitive) and nonlinear load are connected at 0.1 s and disconnected at 0.2 s. Islanding occurs at 0.3 s, and the responses of the frequency and entropy are presented in Fig. 13. From Fig. 13(a) and (b), it is clear that switching of *R* and *L* load does not generate any transient disturbance, and the frequency remains within the thresholds range. While the switching of the *C* load and nonlinear load as presented in Fig. 13(c) and 13(d) produces a transient and deviates the frequency outside the thresholds, which can trip a false islanding detection. Nevertheless, the entropy does not exceed zero during the *C* load and nonlinear load switching, while it becomes positive during islanding. Hence, the second decision criteria based on entropy prevents false islanding tripping. When islanding occurs, both frequency and entropy conditions are verified, and islanding is detected.

E. Performance of the IDM During Voltage Variations and Faults Occurrence

Voltage variations such as sag and swell are common power quality problems in the power system that can occur several times at the PCC bus. Voltage sags are caused by three-phase

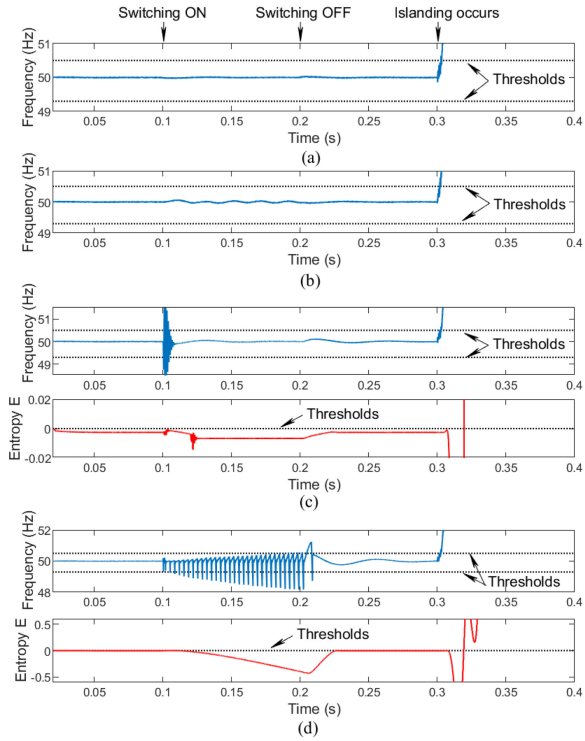

Fig. 13. Proposed IDM under load switching.

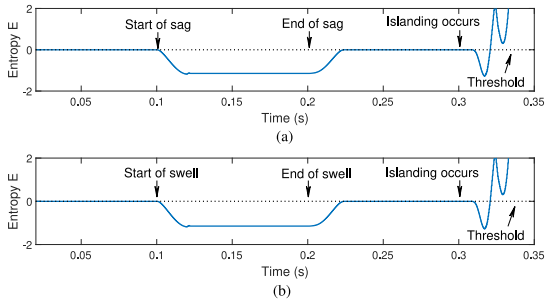

Fig. 14. Response of entropy under voltage sag and swell.

fault, motor starting, or abrupt increases in loads, and voltage swells are caused by damaged neutral connection. If there are voltage variations under such disturbances, the OUV relay should not trip. Therefore, the proposed IDM is tested under voltage variations. The condition of sag and swell (20 % fall and rise in PCC voltage) is simulated at 0.1 s, and it recovers its nominal voltage at 0.2 s. The islanding event is created at 0.3 s. The corresponding entropy responses are presented in Fig. 14. Both sag and swell present the same entropy response, and the disturbance is insignificant compared with the islanding condition. Moreover, it appears that the entropy is negative under sag and swell conditions, while it is moving toward positive values during the islanding condition. Thus, the suggested method can differentiate between islanding and voltage changes.

Similarly, to evaluate the reliability of the suggested scheme under fault conditions, line-to-ground (L–G) and line-to-line (L–L) faults are created between 0.1 and 0.2 s with very small fault impedance equal to $0.1\ \Omega$. The entropy responses are presented

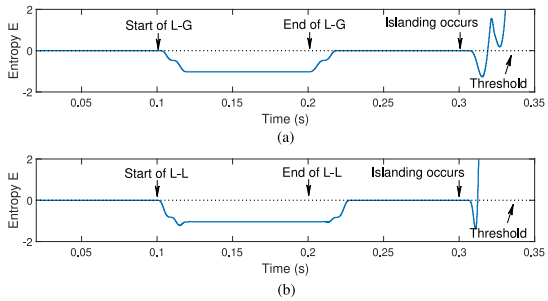

Fig. 15. Entropy response under fault conditions.

TABLE I
COMPARISON RESULTS OF THE SUGGESTED METHOD WITH OTHER STRATEGIES

	Detection time (ms)	NDZ (%)	FDZ (%)
UFP/OFP method	130	46.49	100
Ref. [15]	20	0	100
Ref. [9]	60	5	3
Ref. [30]	55	3	5
Proposed method	20	0	1

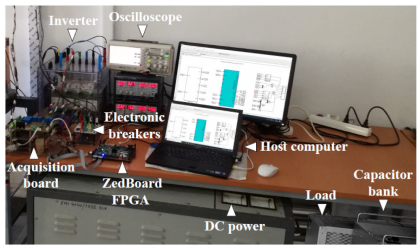

Fig. 16. Overview of the experimental setup.

in Fig. 15. It is obvious from the figure that the entropy extracted is below zero under both faults, and the proposed IDM can avoid false relay tripping.

F. Comparison of the Proposed Method With Other Strategies

The suggested IDM is compared to the previously described approaches such as that stated in [9] and [30]. The comparison is based on detection time, NDZ, and FDZ, and the findings are reported in Table I.

It is concluded from these comparisons that the suggested technique is faster in identifying islanding event, and its NDZ and FDZ are negligible. Moreover, when comparing findings, additional factors should be taken into accounts, such as the number of parameters used for detection as well as the difficulty of implementation.

VI. EXPERIMENTAL VERIFICATION

To test the performance of the proposed method experimentally, a small-scale system is built. Fig. 16 illustrates an overview of the setup. The calculator used in the setup is the ZedBoard field-programmable gate array, and the voltage source inverter is the SemiKron two levels. The DG must be synchronized before being connected to the grid. When the DG and grid voltages are synchronized, the circuit breaker CB, is closed to link the DG to

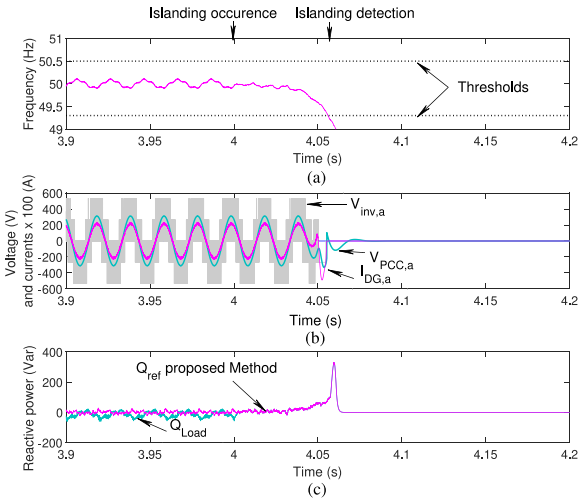

Fig. 17. Experimental waveforms under $\Delta P = 0$.

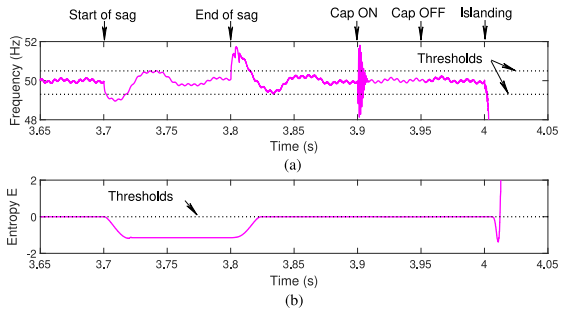

Fig. 18. Experimental waveforms during sag and capacitor switching.

the utility. The sampling frequency is 50 kHz, and the data acquisition is provided via Simulink interface. The system parameters for experimental evaluation are : $P_{\mathrm{DG}} = 1$ kW; $V_{\mathrm{DC}} = 800$ V; $V_g = 220$ V; $R = 145\ \Omega$; $L = 46$ mH; and $C = 22\ \mu$F.

Fig. 17 presents the experimental responses when $\Delta P = 0$ and $Q_f = 1.0$. The rated active power of the DG is 1 kW. The islanding event occurs at 4 s, and the detection time of islanding is 0.06 s as shown in Fig. 17(a), complying with the IEEE 1547-2018 standard's criteria. Fig. 17(b) presents the measured voltage and current waveforms (time-domain) of the inverter and PCC during islanding detection. As may be observed in Fig. 17(b) during the clearing time, the suggested approach does not cause considerable current and voltage distortion due to the positive sequence voltage of the PCC bus in (12). Fig. 17(c) presents the reactive power of the DG and load. The DG reactive power is closely matched with the load's needed reactive power, preventing the injection/drawing of the undesirable reactive power into the utility grid. As a result, the suggested antiislanding approach can identify the islanding condition with zero NDZ.

To assess the proposed IDM's performance practically during the voltage sag and load switching, a 20% voltage sag is created at 3.7 s and ended at 3.8 s, and a capacitor bank of 10 kVar is connected at 3.9 s and disconnected at 3.95 s as depicted in Fig. 18. The islanding event occurs at 4 s, and it is detected

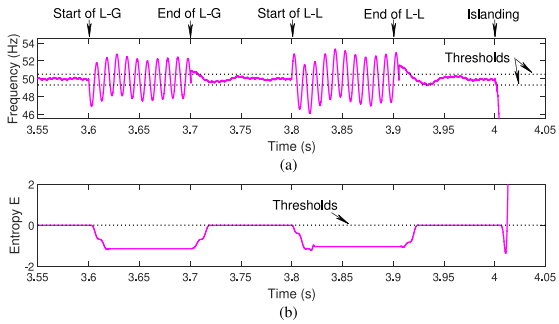

Fig. 19. Experimental waveforms during fault conditions.

within three cycles. Voltage sag and capacitor switching create significant variations on the frequency as presented in Fig. 18(a). These frequency variations surpass the thresholds range, which can issue a false islanding detection. Nevertheless, the suggested algorithm includes a second-level decision-making criterion based on entropy. As observed from Fig. 18(b), the entropy of the voltage sag is small and negative, while in the case of capacitor switching, it is negligible. It is clear from the same figure that the islanding event creates a significant change in entropy that takes positive values. In this case, since both frequency and entropy requirements are met, islanding is identified.

Similarly, the proposed IDM is tested practically under fault conditions. The line-to-ground (L–G) and line-to-line (L–L) faults are created at 3.6 s and 3.8 s, and ended at 3.7 s and 3.9 s, respectively, with negligible fault resistance. As shown in Fig. 19(a), both types of faults deviate the frequency to cross its thresholds range that trips a false islanding detection. Nevertheless, the entropy of both faults is less than zero, avoiding false tripping. When an islanding event occurs, frequency and entropy conditions are verified, and the islanding relay trip. Therefore, the suggested method can distinguish between islanding and nonislanding occurrences and avoid nuisance tripping.

VII. Conclusion

This article proposes a modified RPC for islanding detection with nuisance tripping suppression. To achieve fast detection and avoid reactive power mismatch in normal operating, the positive sequence PCC voltage is incorporated in the reference of the reactive power. Further, to avoid false islanding detection, the wavelet entropy is incorporated into the decision-making criteria, making the IDM more dependable during nuisance tripping. The proposed method may be used to identify any nonislanding situation. It can be concluded that the suggested IDM is fast, offers zero reactive power mismatch during normal operation, and successfully distinguishes between islanding and nonislanding occurrences.

References

[1] T. Quoc-Tuan, "New methods of islanding detection for photovoltaic inverters," in *Proc. IEEE PES Innov. Smart Grid Technol. Conf. Europe*, 2016, pp. 1–5.

[2] F. De Mango, M. Liserre, A. Dell'Aquila, and A. Pigazo, "Overview of anti-islanding algorithms for PV systems. Part I: Passive methods," in *Proc. 12th Int. Power Electron. Motion Control Conf.*, 2006, pp. 1878–1883.
[3] F. De Mango, M. Liserre, and A. Dell'Aquila, "Overview of anti-islanding algorithms for PV systems. Part II: Active methods," in *Proc. 12th Int. Power Electron. Motion Control Conf.*, 2006, pp. 1884–1889.
[4] H. Vahedi, R. Noroozian, A. Jalilvand, and G. B. Gharehpetian, "A new method for islanding detection of inverter-based distributed generation using dc-link voltage control," *IEEE Trans. Power Del.*, vol. 26, no. 2, pp. 1176–1186, Apr. 2011.
[5] F. Liu, Y. Zhang, M. Xue, X. Lin, and Y. Kang, "Investigation and evaluation of active frequency drifting methods in multiple grid-connected inverters," *IET Power Electron.*, vol. 5, no. 4, pp. 485–492, 2012.
[6] A. Timbus, A. Oudalov, and C. N. M. Ho, "Islanding detection in smart grids," in *Proc. IEEE Energy Convers. Congr. Expo.*, 2010, pp. 3631–3637.
[7] M. Khodaparastan, H. Vahedi, F. Khazaeli, and H. Oraee, "A novel hybrid islanding detection method for inverter-based DGs using SFS and ROCOF," *IEEE Trans. Power Del.*, vol. 32, no. 5, pp. 2162–2170, Oct. 2017.
[8] D. Mlakic, H. R. Baghaee, and S. Nikolovski, "Gibbs phenomenon-based hybrid islanding detection strategy for VSC-based microgrids using frequency shift, THD_U, and RMS_U," *IEEE Trans. Smart Grid*, vol. 10, no. 5, pp. 5479–5491, Sep. 2019.
[9] D. Mlakic, H. R. Baghaee, and S. Nikolovski, "A novel ANFIS-based islanding detection for inverter-interfaced microgrids," *IEEE Trans. Smart Grid*, vol. 10, no. 4, pp. 4411–4424, Jul. 2019.
[10] H. R. Baghaee, D. Mlakic, S. Nikolovski, and T. Dragicevic, "Support vector machine-based islanding and grid fault detection in active distribution networks," *IEEE Trans. Emerg. Sel. Topics Power Electron.*, vol. 8, no. 3, pp. 2385–2403, Sep. 2020.
[11] H. R. Baghaee, D. Mlakic, S. Nikolovski, and T. Dragiccvic, "Anti-islanding protection of PV-based microgrids consisting of PHEVs using SVMs," *IEEE Trans. Smart Grid*, vol. 11, no. 1, pp. 483–500, Jan. 2020.
[12] X. Chen and Y. Li, "An islanding detection method for inverter-based distributed generators based on the reactive power disturbance," *IEEE Trans. Power Electron.*, vol. 31, no. 5, pp. 3559–3574, May 2016.
[13] M. Braun, "Reactive power supply by distributed generators," in *Proc. IEEE Power Energy Soc. Gen. Meeting—Convers. Del. Elect. Energy 21st Century*, 2008, pp. 1–8.
[14] H. H. Zeineldin, "A $Q - f$ droop curve for facilitating islanding detection of inverter-based distributed generation," *IEEE Trans. Power Electron.*, vol. 24, no. 3, pp. 665–673, Mar. 2009.
[15] X. Chen and Y. Li, "An islanding detection algorithm for inverter-based distributed generation based on reactive power control," *IEEE Trans. Power Electron.*, vol. 29, no. 9, pp. 4672–4683, Sep. 2014.
[16] P. P. Mishra and C. N. Bhende, "Islanding detection scheme for distributed generation systems using modified reactive power control strategy," *IET Gener., Transmiss. Distrib.*, vol. 13, no. 6, pp. 814–820, 2019.
[17] X. Chen, X. Wang, J. Jian, Z. Tan, Y. Li, and P. Crossley, "Novel islanding detection method for inverter-based distributed generators based on adaptive reactive power control," *J. Eng.*, vol. 2019, no. 17, pp. 3890–3894, 2019.
[18] S. Park, M. Kwon, and S. Choi, "Reactive power P&O anti-islanding method for a grid-connected inverter with critical load," *IEEE Trans. Power Electron.*, vol. 34, no. 1, pp. 204–212, Jan. 2019.
[19] H. H. Zeineldin, E. F. El-Saadany, and M. M. A. Salama, "Impact of DG interface control on islanding detection and nondetection zones," *IEEE Trans. Power Del.*, vol. 21, no. 3, pp. 1515–1523, Jul. 2006.
[20] M. Yingram and S. Premrudeepreechacharn, "Investigation of relationship between voltage and nondetection zone of OUV/OUF of local islanding detection techniques," *J. Clean Energy Technol.*, vol. 2, no. 4, pp. 299–304, 2014.
[21] Wavelet Basis Selection for Transient Signal Analysis of Power Systems. New York, NY, USA: Wiley, 2016, ch. 5, pp. 62–75.
[22] B. Wu, S. Li, K. M. Smedley, and S. Singer, "Analysis of high-power switched-capacitor converter regulation based on charge-balance transient-calculation method," *IEEE Trans. Power Electron.*, vol. 31, no. 5, pp. 3482–3494, May 2016.
[23] A. Samir *et al.*"Wavelet transform applications in power system dynamics," *Elect. Power Syst. Res.*, vol. 83, no. 1, pp. 237–245, 2012.
[24] U. D. Dwivedi and S. N. Singh, "Enhanced detection of power-quality events using intra and interscale dependencies of wavelet coefficients," *IEEE Trans. Power Del.*, vol. 25, no. 1, pp. 358–366, Jan. 2010.
[25] A. Pigazo, M. Liserre, R. A. Mastromauro, V. M. Moreno, and A. Dell Aquila, "Wavelet-based islanding detection in grid-connected PV systems," *IEEE Trans. Ind. Electron.*, vol. 56, no. 11, pp. 4445–4455, Nov. 2009.
[26] C. HwanK. and R. Aggarwal, "Wavelet transforms in power systems. I. General introduction to the wavelet transforms," *Power Eng. J.*, vol. 14, no. 2, pp. 81–87, 2000.
[27] H. Laaksonen, "Novel wavelet transform based islanding detection algorithms," *Int. Rev. Elect. Eng.*, vol. 8, no. 6, pp. 1796–1805, 2013.
[28] S. Mallat, "An approximation tour," in *A Wavelet Tour of Signal Processing*, *2nd ed*. San Diego, CA, USA: Academic, 1999, ch. IX, pp. 376–433.
[29] D. L. Donoho, "De-noising by soft-thresholding," *IEEE Trans. Inf. Theory*, vol. 41, no. 3, pp. 613–627, May 1995.
[30] S. Nikolovski, H. R. Baghaee, and D. Mlakic, "Islanding detection of synchronous generator-based DGs using rate of change of reactive power," *IEEE Syst. J.*, vol. 13, no. 4, pp. 4344–4354, Dec. 2019.

Marouane El Azzaoui was born in Khenifra, Morocco. He received the Engineering degree in electrical engineering from the Faculty of Sciences and Techniques, University of Abdelmalek Essaadi, Tanger, Morocco, in 2012, and the Ph.D. degree in electrical engineering from the Mohammadia School of Engineers, University of Mahamed 5, Rabat, Morocco, in 2018.

He is currently working as a Professor with National School of Applied Sciences of Agadir, Ibn Zohr University, Agadir, Morocco. His research interests include electric power systems, protection and control of microgrids, and applications of power electronics in the power system.

Dr. El Azzaoui is also serving as a reviewer to many reputed international journals.